Spectral Operator Methods for Learning Coherent Temporal Representations in Cellular Signaling Dynamics

Anonymous authors
Paper under double-blind review

Abstract

We present a novel operator-based framework for learning coherent temporal representations of cellular dynamics from live-cell imaging data. Recognizing the inherent stochasticity and measurement limitations in biological systems, our approach shifts the focus from predicting exact trajectories to characterizing key dynamical properties that shape cellular behaviors at the population level. By leveraging spectral analysis of the Koopman operator and smoothing via Markov semigroups of kernel integral operators, we identify near-resonant patterns and transient coherent structures that persist across different experimental conditions. This methodology effectively captures fundamental dynamics, providing insights into mechanisms of heterogeneous cell responses without the need to model precise transformation laws. We demonstrate the efficacy of our framework on a dataset of retinal pigment epithelial cells with an inducible oncogene, revealing conserved dynamical patterns across varying levels of ERK inhibition. Our work offers interpretable learned representations, even with limited and noisy single-cell-resolved recordings, advancing machine learning for dynamical systems and opening new avenues for understanding and predicting cellular behavior in response to external stimuli.

1 Introduction

Understanding complex dynamical behaviors of cellular signaling networks remains a fundamental challenge in computational biology and machine learning Ideker et al. (2001). Unlike engineered systems with deterministic functions and precise equations of motion, cellular dynamics emerge from the interactions of small numbers of molecules whose combinatorial complexity leads to inherent stochasticity Eldar & Elowitz (2010); Altschuler & Wu (2010). More precisely, operating far from thermodynamic limits where large numbers would average out fluctuations, these subcellular systems exhibit pronounced stochastic effects - from spontaneous switching between cellular states to heterogeneous responses to perturbations Elowitz et al. (2002); Spencer et al. (2009).

Factors such as interacting signaling pathways, varying mRNA half-lives, and fluctuating environments contribute to intrinsic stochasticity within genetically identical (isogenic) cell populations Eldar & Elowitz (2010); Altschuler & Wu (2010). Rather than viewing this stochasticity as experimental noise to be filtered out, we recognize it as a fundamental feature that both enables cellular decision-making and induces signatures for identifying robust dynamical patterns Purvis & Lahav (2013); Levine et al. (2013). A striking example is how cells achieve coordination among groups of co-regulated genes (regulons) through noise-driven mechanisms Eldar & Elowitz (2010). These mechanisms operate across multiple scales, from molecular fluctuations that trigger gene expression switches to population-level coordination of cellular states Elowitz et al. (2002). Capturing these complex dynamics is further complicated by limitations in measurement technologies. Traditional high-throughput single-cell technologies enable rapid collection of distributions across diverse conditions Lin et al. (2015; 2016) but lack temporal pairing between cells Weinreb et al. (2018). While live-cell imaging provides time-resolved measurements Cutrale et al. (2017), it is limited to tracking only a few variables simultaneously due to technical constraints Stewart et al. (2016). Consequently, analyzing cellular dynamics from live-cell imaging presents significant challenges due to both intrinsic stochastic fluctuations and extrinsic heterogeneity between cells. This heterogeneity, which

single-cell analysis aims to uncover, makes it particularly difficult to distinguish between transient behaviors and to build predictive models. Current approaches often average out cell-to-cell variations, obscuring the very heterogeneity that single cell data is designed to uncover and only provide phenomenological descriptions without mechanistic insights Snijder & Pelkmans (2011).

While several methods have been developed for analyzing live-cell data, none fully addresses the challenges of modeling cellular dynamics. CODEX (Jacques et al., 2021) employs convolutional neural networks for pattern recognition in time-series data. However, it treats cellular trajectories as static patterns for classification rather than as evolving dynamical systems. While effective at identifying recurring motifs, CODEX does not explicitly model the underlying dynamics or stochastic processes, requires large training datasets, and produces models that are challenging to interpret mechanistically. Functional principal component analysis (fPCA) has been applied to analyze variability in live-cell imaging data (Sampattavanich et al., 2018), particularly for studying temporal changes in molecular concentrations between nucleus and cytoplasm. While fPCA effectively decomposes trajectories into orthogonal modes capturing dominant patterns, its optimization for variance explained rather than dynamical features means these components may not correspond to meaningful biological processes. Moreover, fPCA cannot predict beyond the observed time window as it does not model the generating system, and manual selection of components can introduce bias.

More established tools in system identification have attempted to address similar limitations. Stable linear dynamical systems (LDS) (Boots, 2009) and its extensions for high-dimensional settings (Chen et al., 2017) provide computationally tractable methods through reduced-rank approximations. However, these methods make restrictive assumptions that limit their ability to capture complex nonlinear dynamics. Their linear evolution assumptions cannot capture nonlinear interactions such as transitions present in biological data, their Gaussian noise models may not reflect true stochastic processes, and their dimensionality reduction can discard important dynamical information. In contrast, our operator-based approach using the Koopman framework explicitly models system evolution without linearity assumptions. By lifting nonlinear dynamics into a linear framework through the action on observables, and regularizing through Markov semigroups, we obtain a mathematically rigorous method with provable convergence properties. Rather than relying on predetermined dimensionality reduction, our method adaptively determines relevant modes through spectral analysis of the regularized operator. This allows us to capture rich nonlinear behaviors while maintaining computational tractability and providing theoretical guarantees about convergence to the true dynamics - key features lacking in current approaches.

Operator-theoretic approaches combined with data-driven learning offer a promising alternative by identifying patterns directly from single-cell measurements while preserving the essential heterogeneity that drives cellular decision-making Das & Giannakis (2019); Mezić (2005). Rather than attempting to learn all behaviors, most of which are unpredictable, we focus on identifying coherent temporal patterns that persist for finite times–analogous to studying coherent structures in turbulent flows Mezić (2013). The Koopman operator approach is particularly promising in this context. By representing dynamics through the action on functions, e.g. fluorescent readouts of protein levels, and through spectral analysis, we can identify near-resonances that shape transient responses to perturbations like drug treatments. Our approach combines and extends several powerful concepts:

1. The Koopman operator framework, which enables study of nonlinear dynamics through linear methods while naturally handling stochastic effects Mezić (2005); Das & Giannakis (2019)

2. Kernel methods that transform complex data into spaces where dynamical patterns become apparent Berry et al. (2015)

3. Regularization techniques via Markov semigroups that make infinite-dimensional problems computationally tractable while preserving biologically relevant features Giannakis (2015)

We demonstrate our framework's effectiveness using live-cell imaging data from cells under various perturbations Chen et al. (2023), showing how it captures coherent temporal patterns that persist despite high variability while highlighting condition-specific dynamics.

2 DYNAMICAL SYSTEM REPRESENTATION

In this section, we present our *Operator-Based Dynamics Framework* for learning coherent temporal representations from live-cell trajectory data. By coherent temporal patterns, we refer to robust, recurring, and interpretable structures in the time evolution of the system that persist across different temporal scales and encapsulate the intrinsic organization of the dynamics, such as periodic cycles, stable trends, attracting sets, or patterns of variability. We demonstrate through our results that the coherent patterns significantly enhance the transferability and generalization capability of the constructed models across diverse datasets. We consider the cellular signaling response as a dynamical system characterized by a state space $\mathbb{X} \subseteq \mathbb{R}^d$ and a flow map $\Phi : \mathbb{X} \times \mathbb{T} \to \mathbb{X}$, where $\mathbb{T} \subseteq \mathbb{R}$ represents time. The flow map $\Phi(x, \Delta t) = \Phi^{\Delta t}(x)$ describes the evolution of an initial state $x \in \mathbb{X}$ over time $\Delta t \in \mathbb{T}$, encapsulating the deterministic dynamics of the system. However, due to inherent uncertainties such as molecular noise and environmental fluctuations, the cellular dynamics exhibit stochastic behavior that cannot be fully captured by a deterministic flow map. To model this uncertainty, we consider the state of the system at time t as a random variable X_t with an associated probability distribution over $\mathbb{X}$. The evolution of the system is thus described in terms of the probabilistic transition of states over time.

To model the probabilistic evolution of the system, we introduce the *transition density function* $p_{\Delta t} : \mathbb{X} \times \mathbb{X} \to [0, \infty)$, which describes the probability density of transitioning from state $x \in \mathbb{X}$ at time t to state $y \in \mathbb{X}$ at time $t + \Delta t$. For a measurable subset $\mathbb{A} \subseteq \mathbb{X}$, the probability of the system transitioning from state x to $\mathbb{A}$ over time Δt is given by:

$$\mathbb{P}[\Phi^{\Delta t}(\mathbf{x}_t) \in \mathbb{A} \mid \mathbf{x}_t = x] = \int_{\mathbb{A}} p_{\Delta t}(x, y) \, \mu(dy), \tag{1}$$

where μ is a measure on $\mathbb{X}$, typically the Lebesgue measure when $\mathbb{X}$ is a subset of $\mathbb{R}^d$. The probabilistic evolution of densities over time can be described using the *Perron-Frobenius operator* (also known as the *transfer operator*) $\mathcal{P}^{\Delta t}$. This operator acts on functions $f \in L^1(\mathbb{X}, \mu)$ and describes how a probability density evolves under the dynamics induced by $\Phi^{\Delta t}$. Formally, for a measure space $(\mathbb{X}, \mathcal{B}, \mu)$, where $\mathcal{B}$ is the Borel sigma-algebra on $\mathbb{X}$, and for any measurable subset $\mathbb{A} \in \mathcal{B}$, the Perron-Frobenius operator $\mathcal{P}^{\Delta t} : L^1(\mathbb{X}, \mu) \to L^1(\mathbb{X}, \mu)$ satisfies:

$$\int_{\mathbb{A}} (\mathcal{P}^{\Delta t} f)(x) \, \mu(dx) = \int_{\Phi^{-\Delta t}(\mathbb{A})} f(x) \, \mu(dx). \tag{2}$$

This equation states that the total probability mass in set $\mathbb{A}$ at time $t + \Delta t$ is equal to the total probability mass in the pre-image $\Phi^{-\Delta t}(\mathbb{A})$ at time t, where $\Phi^{-\Delta t}$ denotes the backward flow over time Δt. The operator $\mathcal{P}^{\Delta t}$ is linear and preserves total probability, i.e., if f is a probability density function, so is $\mathcal{P}^{\Delta t} f$. Alternatively, when the transition density function $p_{\Delta t}(x, y)$ exists, the action of the Perron–Frobenius operator can be expressed as:

$$(\mathcal{P}^{\Delta t} f)(y) = \int_{\mathbb{X}} p_{\Delta t}(x, y) f(x) \mu(dx). \tag{3}$$

Koopman Operator: Complementary to the Perron–Frobenius operator, which describes the evolution of densities, the *Koopman operator* $\mathcal{K}^{\Delta t}$ acts on observables (functions of the state) and captures how these observables evolve under the dynamics. Specifically, for an observable function $g \in L^\infty(\mathbb{X}, \mu)$, the Koopman operator $\mathcal{K}^{\Delta t} : L^\infty(\mathbb{X}, \mu) \to L^\infty(\mathbb{X}, \mu)$ is defined as:

$$(\mathcal{K}^{\Delta t} g)(x) = \mathbb{E}[g(\Phi(\mathbf{x}_t)) \mid \mathbf{x}_t = x] = \int_{\mathbb{X}} g(y) p_{\Delta t}(x, y) \, \mu(dy). \tag{4}$$

The Koopman operator is also linear, even if the underlying dynamics are nonlinear and stochastic. It provides a linear representation of the evolution of observables under the dynamics. Moreover, the Koopman operator is the adjoint of the Perron-Frobenius operator with respect to the inner product in $L^2(\mathbb{X}, \mu)$, i.e., for $f \in L^1(\mathbb{X}, \mu)$ and $g \in L^\infty(\mathbb{X}, \mu)$,

$$\int_{\mathbb{X}} (\mathcal{K}^{\Delta t} g)(x) f(x) \, \mu(dx) = \int_{\mathbb{X}} g(x) (\mathcal{P}^{\Delta t} f)(x) \, \mu(dx). \tag{5}$$

This duality allows us to study the dynamics either through the evolution of densities (Perron-Frobenius operator) or through the evolution of observables (Koopman operator).

2.1 Spectral Analysis of the Koopman Operator

As a linear operator, the Koopman operator $\mathcal{K}^{\Delta t}$ can be decomposed into its eigenfunctions and eigenvalues. Specifically, we seek eigenfunctions $\phi_k \in L^\infty(\mathbb{X}, \mu)$ and corresponding eigenvalues $\lambda_k \in \mathbb{C}$ satisfying:

$$\mathcal{K}^{\Delta t} \phi_k = \lambda_k \phi_k. \tag{6}$$

These eigenfunctions represent modes of the system that evolve linearly over time. By approximating these eigenfunctions and eigenvalues, we can decompose complex, nonlinear, and stochastic dynamics into a superposition of simpler, linear modes.

Pseudospectra of the Koopman: Given the stochastic and transient nature of cellular dynamics and the limitations in predicting exact trajectories, we adopt a *pseudospectrum approach* to identify coherent dynamical patterns that are robust to perturbations and uncertainties. The ϵ-pseudospectrum of the Koopman operator $\mathcal{K}^{\Delta t}$, denoted by $\sigma_\epsilon(\mathcal{K}^{\Delta t})$, consists of all complex numbers $\lambda \in \mathbb{C}$ for which the resolvent norm is large:

$$\sigma_\epsilon(\mathcal{K}^{\Delta t}) = \left\{ \lambda \in \mathbb{C} \ \middle| \ \left\| \left(\mathcal{K}^{\Delta t} - \lambda I \right)^{-1} \right\| \geq \frac{1}{\epsilon} \right\}. \tag{7}$$

However, working directly with resolvents can be computationally challenging (Sharma et al., 2016; Giannakis & Valva, 2024; Colbrook & Townsend, 2021; Colbrook et al., 2023). Therefore, in the subsequent sections, we adopt an alternative approach to analyze finite-time dynamics and transient behaviors by employing a method based on smoothing via a Markov semigroup of kernel integral operators (Valva & Giannakis, 2024). While this approach may not yield the exact pseudospectrum due to the regularization of the Koopman operator, the eigenfunctions of the smoothed operator still represent coherent temporal patterns that persist over finite timescales. While this approach yields a different spectrum from the original Koopman operator or its pseudospectrum, it effectively captures near-resonant behaviors and coherent transient patterns in the dynamics, similar to the pseudospectrum approach.

Identification of Coherent Dynamical Patterns Approximate eigenfunctions obtained from the smoothing method represent coherent temporal patterns in the cellular dynamics that persist over finite timescales. These patterns evolve nearly linearly and can be used to decompose the complex dynamics into a sum of simpler, predictable components. For an approximate eigenfunction ϕ_j, the evolution under the Koopman operator satisfies:

$$\mathcal{K}^{n\Delta t} g \approx \lambda^n g, \tag{8}$$

for $n \in \mathbb{N}$. This approximation holds over finite timescales where the patterns remain coherent. By expressing observables as linear combinations of these approximate eigenfunctions, we obtain a spectral decomposition of the dynamics:

$$g(x) = \sum_j \phi_j(x) c_j, \tag{9}$$

where ϕ_j are the approximate eigenfunctions and c_j are coefficients. The evolution of g is then approximated by:

$$\mathcal{K}^{n\Delta t} g(x) \approx \sum_j \lambda_j^n \phi_j(x) c_j. \tag{10}$$

This decomposition allows us to capture the dominant temporal patterns in the data, even when exact trajectory prediction is impossible. The approximate eigenfunctions ϕ_j correspond to modes that represent collective behaviors of the system, providing insights into the mechanisms underlying cellular responses.

2.2 Learning the Spectral Components of the Dynamics

To extract coherent temporal patterns from live-cell trajectory data, we employ a data-driven approach to approximate the Koopman operator. Before detailing the approximation method, we first describe the data and the experimental conditions under which it was collected.

Experimental Conditions Let $\{C_k\}_{k=1}^K$ denote the different experimental conditions under which live-cell imaging data were collected. Each condition C_k represents a specific perturbation or treatment applied to the cells, such as varying doses of an inhibitor or other perturbations. For each condition, we observe N_k cell trajectories, where each trajectory consists of time-series measurements over T time points. The measurements are denoted by $\{x_t^{(i,k)}\}_{t=0}^T$ for the i-th cell in condition C_k, where $x_t^{(i,k)} \in \mathbb{R}^d$ represents the state vector of observable quantities (e.g., fluorescence intensities corresponding to signaling molecule activities) at time t.

Delay-Coordinate Embedding To capture the underlying dynamics of the system and obtain a data-informed geometry suitable for constructing a Markov operator, we employ delay-coordinate embedding. This method reconstructs the phase space of the dynamical system using time-delayed observations of the measured variables, effectively unfolding the dynamics into a higher-dimensional space (Takens, 1996). For each trajectory, we construct a delay-coordinate map $F_Q : \mathbb{X} \to \mathbb{R}^{Qd}$ defined by

$$F_Q(x_t) = \left[x_t^\top, x_{t-\Delta t}^\top, x_{t-2\Delta t}^\top, \ldots, x_{t-(Q-1)\Delta t}^\top \right]^\top, \tag{11}$$

where Q is the number of delays and Δt is the sampling interval. The delay-coordinate embedding captures the temporal structure of the data, allowing us to reconstruct the dynamics even when only a few variables are measured.

Kernel Function and Integral Operator Using the embedded data, we define a kernel function $k : \mathbb{R}^{Qd} \times \mathbb{R}^{Qd} \to \mathbb{R}_+$ to quantify the similarity between points. We employ a self-tuning kernel that adapts to the local data density (Berry & Harlim, 2016):

$$k(x,y) = \exp\left(-\frac{\|x-y\|^2}{\sigma(x)\sigma(y)} \right), \tag{12}$$

where $\|\cdot\|$ denotes the Euclidean norm, and $\sigma(x)$ is a local bandwidth parameter. This kernel captures local structures while being robust to variations in data density.

We then construct an integral operator K acting on functions $f : \mathbb{R}^{Qd} \to \mathbb{R}$:

$$(Kf)(x) = \int_{\mathbb{R}^{Qd}} k(x,y) f(y) \, d\mu(y), \tag{13}$$

where μ is the empirical measure derived from the data.

Markov Operator and Eigenvalue Problem To analyze the dynamics in probability spaces, we normalize the kernel to construct a Markov operator. The normalization involves computing the degree function

$$d(x) = \int_{\mathbb{R}^{Qd}} k(x,y) \, d\mu(y), \tag{14}$$

and then normalizing the kernel:

$$\tilde{k}(x,y) = \frac{k(x,y)}{d(x)}. \tag{15}$$

The normalized kernel defines a Markov operator P:

$$(Pf)(x) = \int_{\mathbb{R}^{Qd}} \tilde{k}(x,y) f(y) \, d\mu(y). \tag{16}$$

This Markov operator P forms the basis for constructing the Markov semigroup P_τ, parameterized by $\tau > 0$, which we will use for smoothing in our spectral approximation. In discrete form, for N data points $x_{i\ i=1}^N$, the Markov matrix P has entries:

$$P_{ij} = \frac{K_{ij}}{\left(\sum_{k=1}^N K_{ik} q_k^{-1/2} \right) q_j^{1/2}}, \quad q_i = \sum_{k=1}^N K_{ik} \tag{17}$$

We compute the eigenvalues γ_j and corresponding eigenvectors φ_j of P by solving the eigenvalue problem:

$$P\varphi_j = \lambda_j\varphi_j. \tag{18}$$

The eigenvalues are real and satisfy $1 = \gamma_1 \geq \gamma_2 \geq \cdots \geq \gamma_N \geq -1$. The leading eigenvector φ_1 corresponds to the stationary distribution of the Markov chain. These eigenvectors φ_j will serve as the basis for our Galerkin approximation of the smoothed Koopman operator.

Sparse Representation To handle large datasets efficiently, we construct a k-nearest neighbor graph to sparsify the kernel matrix. For each data point x_i, we connect it to its k nearest neighbors based on the Euclidean distance in the embedded space. The kernel function is then applied only to these neighboring pairs, resulting in a sparse kernel matrix K and, consequently, a sparse Markov matrix P. This sparsity reduces computational complexity and storage requirements, making the method scalable to large datasets. While the Markov operator P captures the dynamics of the system, direct spectral analysis may be sensitive to noise and perturbations. To address this, we introduce a smoothing approach using a Markov semigroup, which will be detailed in the following Galerkin approximation section.

Markov Semigroup for Smoothing To enhance the robustness of our spectral analysis to noise and perturbations, we introduce a Markov semigroup P_τ. This semigroup is generated by the Markov operator P and is defined for $\tau \geq 0$ as:

$$P_\tau = e^{\tau(P-I)}, \tag{19}$$

where I is the identity operator. The semigroup satisfies the properties: $P_0 = I$, $P_{\tau_1}P_{\tau_2} = P_{\tau_1+\tau_2}$ for all $\tau_1, \tau_2 \geq 0$ and strongly continuous at 0, i.e. $\lim_{\tau \to 0^+} |P_\tau f - f| = 0$ for all f in the domain of P.

The parameter τ controls the amount of smoothing: as τ increases, P_τ becomes increasingly diffusive, smoothing out fine-scale features in the data.

Galerkin Approach and Smoothing by Markov Semigroup To approximate the Koopman operator and its eigenfunctions, we employ a Galerkin method (Rowley et al., 2009; Klus, 2020) incorporating smoothing by a Markov semigroup of kernel integral operators (Valva & Giannakis, 2024). We project the smoothed Koopman operator onto the subspace spanned by the leading L eigenvectors of the Markov operator P, denoted as $\{\varphi_j\}_{j=1}^L$. The smoothing process is achieved through the application of the Markov semigroup P_τ, parameterized by $\tau > 0$. We approximate the eigenfunctions of the smoothed operator as linear combinations:

$$\phi_\tau = \sum_{j=1}^L c_j\varphi_j. \tag{20}$$

The coefficients c_j are determined by enforcing that the action of the smoothed Koopman operator on ϕ_τ is approximated within the chosen subspace. Specifically, we consider the finite-dimensional approximation of the smoothed Koopman operator $\mathbf{K}_\tau$, defined by:

$$\mathbf{K}_\tau = \mathbf{G}^{-1}\mathbf{A}_\tau, \tag{21}$$

where $\mathbf{G}$ is the Gram matrix and $\mathbf{A}_\tau$ is the smoothed covariance matrix, with entries:

$$G_{ij} = \langle \varphi_i, \varphi_j \rangle, \quad A_{\tau,ij} = \langle \varphi_i, P_{\tau/2}\mathcal{K}P_{\tau/2}\varphi_j \rangle. \tag{22}$$

Here, $P_{\tau/2}$ represents the action of the Markov semigroup, which smooths the Koopman operator. The inner product $\langle \cdot, \cdot \rangle$ is approximated using the empirical data as before.

To compute the entries of $\mathbf{A}_\tau$, we approximate the action of the smoothed Koopman operator on the basis functions using the time-series data and the kernel integral operator. Assuming that x_{n+1} follows x_n in the data, we have:

Algorithm 1 Koopman Eigenfunction Approximation

Require: Time series $\{x_k\} \in \mathbb{R}^d$, delays Q, neighbors k_{nn}, Markov eigenfunctions $l \leq N$, regularization $\theta \geq 0$, output dim $l' \leq l$

Ensure: Koopman eigenvalues $\{\lambda_k\}_{k=1}^{l'} \in \mathbb{C}$, frequencies $\{\omega_k\}_{k=1}^{l'} \in \mathbb{R}$, eigenfunctions $\{\psi_k\}_{k=1}^{l'} \in \mathbb{C}^N$

1: Compute pairwise distances $d_Q^2(x_i, x_j) = \frac{1}{Q} \sum_{k=0}^{Q-1} \| x_{i-k} - x_{j-k} \|^2$
2: Retain k_{nn} nearest neighbors for each point i in set $\mathcal{N}_{k_{nn}}(x_i)$
3: Symmetrize distances by augmenting if $x_i \in \mathcal{N}_{k_{nn}}(x_j)$ but $x_j \notin \mathcal{N}_{k_{nn}}(x_i)$
4: Compute bandwidth $\epsilon(x_i, x_j)$ (Berry & Harlim, 2016)
5: Form kernel matrix $K_{ij} = \exp(-d_Q^2(x_i, x_j)/\epsilon)$
6: Compute normalized matrix $P_{ij} = K_{ij}/(\sum_k K_{ik} q_k^{-1/2}) q_j^{1/2}, q_i = \sum_k K_{ik}$
7: Find l largest eigenvalues γ_k and eigenfunctions φ_k of P
8: Form Galerkin matrices $A_{ij} = \langle \varphi_i, V\xi_j \rangle - \theta \langle \varphi_i, \Delta\xi_j \rangle, G_{ij} = \langle \varphi_i, \xi_j \rangle$
9: Solve $Ac = \lambda Gc$ for coefficients c_k and eigenvalues λ_k
10: Compute eigenfunctions $\psi_i = \sum_{j=1}^{l} c_{ji} \varphi_j$
11: Calculate Dirichlet energies $E(\psi_i) = \langle \psi_i, \Delta\psi_i \rangle / \|\psi_i\|^2$
12: Order (λ_k, ψ_k) by increasing $E(\psi_k)$
13: Compute frequencies $\omega_k = \text{Im}(\lambda_k)$

$$(P_{\tau/2}\mathcal{K}P_{\tau/2}\varphi_j)(x_n) \approx \int \tilde{k}_{\tau/2}(x_n, y)\varphi_j(y_{n+1})d\mu(y), \tag{23}$$

where $\tilde{k}_{\tau/2}$ is the normalized kernel function associated with $P_{\tau/2}$. Thus, the entries of $\mathbf{A}_\tau$ become:

$$A_{\tau,ij} = \frac{1}{N} \sum_{n=1}^{N-1} \varphi_i(x_n) \int \tilde{k}_{\tau/2}(x_n, y)\varphi_j(y_{n+1})d\mu(y). \tag{24}$$

Solving the generalized eigenvalue problem

$$\mathbf{A}_\tau c = \lambda\mathbf{G}c, \tag{25}$$

yields approximations of the eigenvalues λ and eigenfunctions ϕ_τ of the smoothed Koopman operator. This approach allows us to extract coherent dynamical patterns that are robust to perturbations and noise, while still capturing the essential features of the underlying dynamics.

Computational Considerations   This approach enables the efficient handling of large datasets by optimizing computational resources. In Algorithm 1, the most computationally intensive steps are the calculation of the kernel matrix K_{ij} (step 5) and the solution of two eigenvalue problems: one for P (step 7) and another for the Galerkin solution (step 9). By employing sparse representations—such as moderating the nearest neighbors k_{nn}—and limiting the number of eigenfunctions l, we effectively reduce the computational burden of the eigenvalue problems while preserving the system's essential dynamics. What facilitates effective work with a limited number of modes is the fact that the extracted eigenfunctions represent intrinsic dynamical patterns, allowing just a few of them to capture the system's dynamical behavior effectively. Additionally, by managing the kernel matrix K_{ij} using techniques like random Fourier features (Giannakis et al., 2023), we can scale kernel computations with the size of the data. This results in a highly efficient computational approach, offering significantly faster training compared to contemporary deep learning and neural network methods while maintaining robust performance in capturing the system's dynamics (Tavasoli et al., 2023).

3   RESULTS

In this section, we apply our spectral operator-based framework to live-cell imaging data to extract coherent temporal patterns in cellular dynamics. We begin by describing the dataset and performing

a preliminary analysis to understand the divergence of cellular trajectories under different experimental conditions. We then demonstrate how our framework captures these dynamics and evaluate the representation performance in reconstructing and predicting ERK activity trajectories. The pseudo-code used to generate the Koopman results is reported in Algorithm 1.

3.1 PRELIMINARY ANALYSIS

Dataset Description   We applied our methodology to a live-cell imaging dataset of retinal pigment epithelial (RPE) cells engineered with a doxycycline (DOX)-inducible $BRAF^{V600E}$ oncogene (Chen et al., 2023). The $BRAF^{V600E}$ mutation is known to activate the mitogen-activated protein kinase (MAPK) signaling pathway, leading to increased extracellular signal-regulated kinase (ERK) activity, which plays a crucial role in cell proliferation and differentiation. The cells were also engineered to express the ERK activity reporter EKAREN5 and a cell cycle indicator (mCherry-dE2F PIP). This setup allowed simultaneous monitoring of ERK signaling dynamics and cell cycle progression. Live-cell imaging was performed every 10 minutes over a period of four days, capturing the temporal evolution of ERK activity in individual cells.

To investigate the effect of ERK inhibition on cellular dynamics, the experiment included varying concentrations of the ERK inhibitor SCH772984 (ERKi). We focused on three experimental conditions:

1. DOX + DMSO: Cells induced with DOX without ERK inhibition (control condition).
2. DOX + Low ERKi: Cells induced with DOX and treated with a low concentration of ERK inhibitor.
3. DOX + High ERKi: Cells induced with DOX and treated with a high concentration of ERK inhibitor.

These conditions allowed us to study how varying levels of ERK inhibition affect the dynamics of ERK activity and cellular responses.

3.2 APPLICATION OF OPERATOR-BASED REPRESENTATION FOR SUBCELLULAR DYNAMICS

We applied our spectral operator-based dynamics framework to the live-cell imaging data to represent coherent temporal patterns and model the dynamics of ERK activity under the different experimental conditions.

Kernel Operator and Block Structure   Using the delay-coordinate embedding with Q delays, we constructed the kernel matrix for the **DOX + Low ERKi** condition. The self-tuning kernel function captured the similarities between data points in the embedded space, and the resulting kernel matrix exhibited a distinct block-diagonal structure, as shown in Figure **??**.

where the block-diagonal structure of the kernel matrix suggests the presence of distinct dynamical regimes or attractors in the cellular state space. This implies that cells transition between different states over time, and these transitions are captured by the coherent patterns in the data.

Principal Koopman Modes   The extracted principal Koopman modes capture the dominant temporal patterns in the ERK signaling dynamics at the level of individual cells. Figure **??** displays the first two Koopman modes obtained under the Low ERKi condition. The **first Koopman mode** describes a smooth shift over time, suggesting a state transition within individual cells. This shift likely reflects the progressive inhibition of ERK activity due to the introduction of the ERK inhibitor. The mode captures the
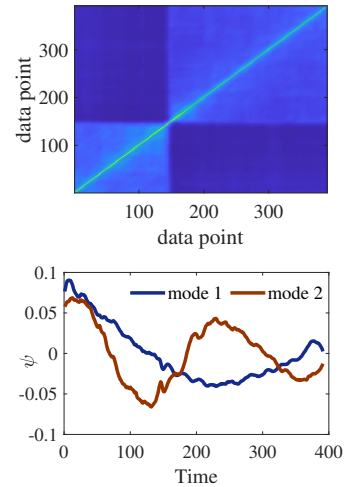

Figure 1: *(top) Kernel operator matrix showing block-diagonal structure, indicating distinct dynamical regimes. (bottom) The first two principal Koopman modes extracted from the data.*

overarching trend of cells moving from a state of high ERK activity to a suppressed state, aligning

with known mechanisms where cells adjust their signaling pathways in response to external perturbations (Eldar & Elowitz, 2010). This collective response demonstrates how cells probabilistically shift states in response to external cues—a hallmark of stochastic differentiation systems. The **second Koopman mode** exhibits oscillatory behavior, alternating between positive and negative values periodically. This pattern indicates the presence of intrinsic cyclical dynamics within the ERK signaling network, possibly related to fluctuations inherent in cellular processes with low copy number molecules (Elowitz et al., 2002). Such oscillations may correspond to cell cycle phases or other regulatory feedback loops that generate transient responses.

Model Reconstruction and Predictions Utilizing a sparse representation with only the 10 smoothest modes, we constructed a model to represent the individual cell ERK activity trajectories. This approach acknowledges the inherent stochasticity in cellular signaling by focusing on the most significant modes that capture essential dynamics while filtering out less predictable variations. We evaluated the model's performance on both the training set (Low ERKi condition) and unseen data—including data after frame 400 in the Low ERKi condition (with one frame every 10 minutes).

TRAINING SET PERFORMANCE   Figure 2 (the left plot) compares the model predictions with the observed ERK activity data for a randomly chosen cell under the Low ERKi condition. The model effectively captures the overall trends and key fluctuations in ERK activity, demonstrating a close match with the observed trajectory. This indicates that the dominant Koopman modes effectively encapsulate both the deterministic response to the inhibitor and the stochastic variations arising from intrinsic noise. By reconstructing the dynamics using a limited number of modes, the framework demonstrates its capacity to distill complex, noisy biological data into interpretable and predictive components.
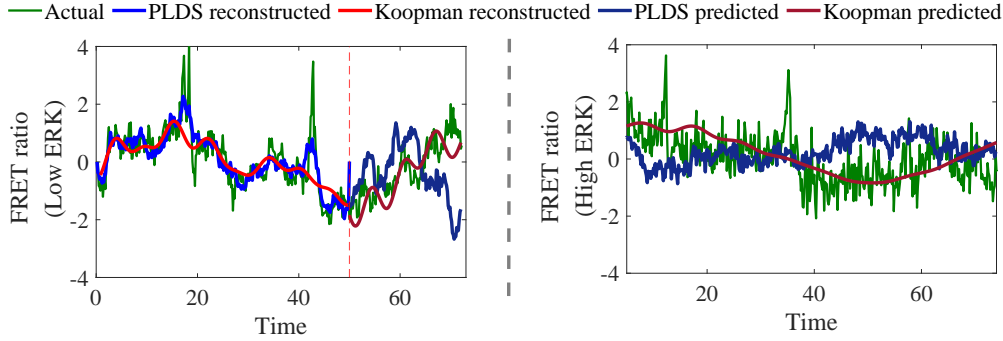

Figure 2: *Performance examples of model prediction for ERK activity trajectories in the Low ERKi condition (**left**, training set) and High ERKi condition (**right**, test set).*

GENERALIZATION TO UNSEEN DATA   We applied the model trained on the Low ERKi condition to the High ERKi condition without retraining, as shown in Figure 2 (right). The model predictions (red) align well with the observed data (green), capturing the general behavior of ERK activity under a higher level of inhibition. Despite the increased perturbation, the principal Koopman modes learned from the Low ERKi data remain relevant, suggesting that the fundamental dynamics of ERK signaling persist across different inhibition levels. This model transfer property is absent in modern approaches like PLDS, as illustrated in Figure 2.

This generalization implies that the Koopman eigenfunctions encapsulate conserved patterns in the cellular response, reflecting core mechanisms of how cells adapt to varying degrees of external stress. The persistence of these modes across conditions indicates that our framework effectively identifies the underlying structures governing the stochastic and nonlinear dynamics of ERK signaling. By capturing these essential features, the model enhances its applicability to various experimental conditions, offering a robust tool for understanding and predicting cellular behavior in response to different perturbations.

COMPARISON OF DIFFERENT METRICS   A comprehensive comparison of different metrics with two contemporary approaches, i.e., CODEX (Jacques et al., 2021) and PLDS (Chen et al., 2017), is seen in Table 1. In predicting cell dynamics, capturing intricate temporal behaviors is essential for understanding complex biological processes. While CODEX may show lower average error, its inability to represent detailed dynamic variations limits their utility in applications requiring high fidelity in transient behaviors. The inconsistent behavior of CODEX becomes apparent when comparing its predictions for LowERKi and HighERKi in Table 1. Intuitively, CODEX should perform more accurately on the seen dataset (LowERKi) than on the unseen dataset (HighERKi). However, the results in Table 1 do not reflect this anticipated trend, raising questions about the method's consistency. The Koopman-based method, by contrast, excels in capturing these fine-grained dynamics, providing deeper insights into cell behavior and enhancing the predictive accuracy for applications where such precision is critical. The datasets were also analyzed using fPCA, which highlighted the advantages of the Koopman operator in capturing intrinsic dynamical modes. However, fPCA is omitted from Table 1 because it lacks predictive or forecasting capabilities. Its primary role is to describe observed variation, offering insights into existing patterns rather than enabling forward-looking predictions.

Table 1: Performance Metrics comparison in heldout data for LowERKi and unseen data for High-ERKi Tests

Metric	Koopman		CODEX (Jacques et al., 2021)		PLDS (Chen et al., 2017)	
	LowERKi	HighERKi	LowERKi	HighERKi	LowERKi	HighERKi
RMSE	1.00(0.37)	1.16(0.26)	1.04(0.42)	0.82(0.31)	1.45(0.48)	1.70(0.46)
MAE	0.78(0.27)	1.00(0.28)	0.81(0.33)	0.67(0.26)	1.18(0.43)	1.42(0.43)
MAPE (%)	448(1742)	382(465)	672(2074)	387(418)	1233(4482)	870(150)
R-squared	-1.08(3.20)	-4.31(6.06)	-1.16(2.68)	-1.70(4)	-7.50(24.34)	-11.44(15.39)
DTW Distance	62(23)	317(96)	61(26)	50(21)	68(33)	295(105)

Implications and Further Considerations   In cells expressing the mutated oncogene $BRAF^{V600E}$, the ERK pathway plays a critical role in regulating cell proliferation and survival. The signaling in these cells can be highly variable due to intrinsic stochasticity and the activation of alternative pathways, leading to heterogeneous cell decisions. When ERK inhibition is absent, as in the DOX + DMSO condition, cells may exhibit increased variability that is not captured by the Koopman modes derived from the ERK-inhibited condition. This variability results in dynamics that require additional modes or joint analysis methods to fully capture. In future work, we plan to incorporate the *Jointly Smooth Functions* method across all conditions with $BRAF^{V600E}$ expression to aid in identifying shared patterns and separating different activated mechanisms (Sroczynski et al., 2024). By integrating data from multiple conditions and employing joint analysis techniques, we aim to enhance the model's ability to capture the full range of cellular behaviors, especially when different signaling pathways are involved. This approach will allow us to account for the complex interplay between pathways and the stochastic nature of cellular signaling, providing a more comprehensive understanding of how cells adapt and make decisions in varying environments. By leveraging these methods in future studies, we expect to better capture the dynamics in conditions where the signaling is highly variable and heterogeneous, such as in the absence of ERK inhibition. This will not only improve the predictive power of our models but also deepen our insight into the fundamental mechanisms driving cellular responses, particularly in systems where noise plays a significant functional role.

4   CONCLUSION

In this study, we developed a spectral operator-based framework that extracts coherent temporal patterns from live-cell trajectory data to represent cellular responses to perturbations. Our findings demonstrate that conserved temporal patterns exist within cellular dynamics, even amidst the inherent stochasticity and variability of biological systems. By focusing on probabilistic representations and utilizing Koopman eigenfunctions, our framework effectively captures fundamental aspects of the dynamics that persist across varying external conditions, providing meaningful insights into complex biological processes. Compared to approaches using functional data analysis or

deep learning architectures, our framework offers significant advantages. It provides interpretable representations through Koopman eigenfunctions, corresponding to meaningful temporal patterns in the data, unlike black-box models. Additionally, it operates efficiently with the limited variables measured in live-cell imaging, addressing common data limitations in biological experiments. By capturing conserved dynamical patterns and accounting for stochasticity, our approach contributes to a deeper comprehension of the mechanisms underlying cellular decision-making and adaptation.

REFERENCES

Steven J Altschuler and Lani F Wu. Cellular heterogeneity: do differences make a difference? *Cell*, 141(4):559–563, 2010.

Tyrus Berry and John Harlim. Variable bandwidth diffusion kernels. *Applied and Computational Harmonic Analysis*, 40(1):68–96, 2016. ISSN 1063-5203. doi: https://doi.org/10.1016/j.acha.2015.01.001. URL https://www.sciencedirect.com/science/article/pii/S1063520315000020.

Tyrus Berry, Dimitrios Giannakis, and John Harlim. Nonparametric forecasting of low-dimensional dynamical systems. *Physical Review E*, 91(3):032915, 2015.

Byron Boots. Learning stable linear dynamical systems. *Online]. Avail.: https://www. ml. cmu. edu/research/dap-papers/dap_boots. pdf [Accessed 30 05 2016]*, 2009.

Jia-Yun Chen, Clemens Hug, José Reyes, Chengzhe Tian, Luca Gerosa, Fabian Fröhlich, Bas Ponsioen, Hugo JG Snippert, Sabrina L Spencer, Ashwini Jambhekar, Peter K. Sorger, and Galit Lahav. Multi-range erk responses shape the proliferative trajectory of single cells following oncogene induction. *Cell reports*, 42(3), 2023.

Shaojie Chen, Kai Liu, Yuguang Yang, Yuting Xu, Seonjoo Lee, Martin Lindquist, Brian S Caffo, and Joshua T Vogelstein. An m-estimator for reduced-rank system identification. *Pattern recognition letters*, 86:76–81, 2017.

Matthew J. Colbrook and Alex Townsend. Rigorous data-driven computation of spectral properties of koopman operators for dynamical systems. *arXiv:2111.14889v1*, pp. 1–45, 2021. doi: arXiv: 2111.14889v1. URL arXiv:2111.14889v1.

Matthew J. Colbrook, Lorna J. Ayton, and Máté Szőke. Residual dynamic mode decomposition: robust and verified koopmanism. *Journal of Fluid Mechanics*, 955:A21, 2023. doi: 10.1017/jfm.2022.1052.

Francesco Cutrale, Vikas Trivedi, Le A Trinh, Chi-Li Chiu, John M Choi, Marcela S Artiga, and Scott E Fraser. Hyperspectral phasor analysis enables multiplexed 5d in vivo imaging. *Nature methods*, 14(2):149–152, 2017.

Suddhasattwa Das and Dimitrios Giannakis. Delay-coordinate maps and the spectra of koopman operators. *Journal of Statistical Physics*, 175(6):1107–1145, 2019.

Avigdor Eldar and Michael B Elowitz. Functional roles for noise in genetic circuits. *Nature*, 467 (7312):167–173, 2010.

Michael B Elowitz, Arnold J Levine, Eric D Siggia, and Peter S Swain. Stochastic gene expression in a single cell. *Science*, 297(5584):1183–1186, 2002.

Dimitrios Giannakis. Dynamics-adapted cone kernels. *SIAM Journal on Applied Dynamical Systems*, 14(2):556–608, 2015. doi: 10.1137/140954544. URL https://doi.org/10.1137/140954544.

Dimitrios Giannakis and Claire Valva. Consistent spectral approximation of koopman operators using resolvent compactification. *Nonlinearity*, 37(7):075021, 2024.

Dimitrios Giannakis, Amelia Henriksen, Joel A. Tropp, and Rachel Ward. Learning to forecast dynamical systems from streaming data. *SIAM Journal on Applied Dynamical Systems*, 22(2):527–558, 2023. doi: 10.1137/21M144983X. URL https://doi.org/10.1137/21M144983X.

Trey Ideker, Timothy Galitski, and Leroy Hood. A new approach to decoding life: systems biology. *Annual review of genomics and human genetics*, 2(1):343–372, 2001.

Marc-Antoine Jacques, Maciej Dobrzyński, Paolo Armando Gagliardi, Raphael Sznitman, and Olivier Pertz. Codex, a neural network approach to explore signaling dynamics landscapes. *Molecular systems biology*, 17(4):e10026, 2021.

Stefan Klus. Data-driven analysis of complex dynamical systems. 2020.

Douglas A Levine, Cancer Genome Atlas Research Network Genome sequencing centres: Broad Institute Getz Gad 1 Gabriel Stacey B. 1 Cibulskis Kristian 1 Lander Eric 1 Sivachenko Andrey 1 Sougnez Carrie 1 Lawrence Mike 1, Washington University in St Louis Kandoth Cyriac 2 Dooling David 2 Fulton Robert 2 Fulton Lucinda 2 Kalicki-Veizer Joelle 2 McLellan Michael D. 2 O'Laughlin Michelle 2 Schmidt Heather 2 Wilson Richard K. 2 Ye Kai 2 Ding Li 2 Mardis Elaine R. 2, University of Southern California & Johns Hopkins Baylin Stephen B. 21 Bootwalla Moiz S. 22 Lai Phillip H. 22 Triche Jr Timothy J. 22 Van Den Berg David J. 22 Weisenberger Daniel J. 22 Laird Peter W. 22 Shen Hui 22, Institute for Systems Biology Reynolds Sheila M. 23 Shmulevich Ilya 23, et al. Integrated genomic characterization of endometrial carcinoma. *Nature*, 497(7447):67–73, 2013.

Jia-Ren Lin, Mohammad Fallahi-Sichani, and Peter K Sorger. Highly multiplexed imaging of single cells using a high-throughput cyclic immunofluorescence method. *Nature communications*, 6(1): 1–7, 2015.

Jia-Ren Lin, Mohammad Fallahi-Sichani, Jia-Yun Chen, and Peter K Sorger. Cyclic immunofluorescence (cycif), a highly multiplexed method for single-cell imaging. *Current protocols in chemical biology*, 8(4):251–264, 2016.

Igor Mezić. Spectral properties of dynamical systems, model reduction and decompositions. *Nonlinear Dynamics*, 41:309–325, 2005. doi: 10.1007/s11071-005-2824-x.

Igor Mezić. Analysis of fluid flows via spectral properties of the koopman operator. *Annual Review of Fluid Mechanics*, 45(1):357–378, 2013. doi: 10.1146/annurev-fluid-011212-140652.

Jeremy E Purvis and Galit Lahav. Encoding and decoding cellular information through signaling dynamics. *Cell*, 152(5):945–956, 2013.

Clarence W. Rowley, Igor Mezić, Shervin Bagheri, Philipp Schlatter, and Dan S. Henningson. Spectral analysis of nonlinear flows. *Journal of Fluid Mechanics*, 641:115–127, 2009. doi: 10.1017/S0022112009992059.

Somponnat Sampattavanich, Bernhard Steiert, Bernhard A Kramer, Benjamin M Gyori, John G Albeck, and Peter K Sorger. Encoding growth factor identity in the temporal dynamics of foxo3 under the combinatorial control of erk and akt kinases. *Cell systems*, 6(6):664–678, 2018.

Ati S Sharma, Igor Mezić, and Beverley J McKeon. Correspondence between koopman mode decomposition, resolvent mode decomposition, and invariant solutions of the navier-stokes equations. *Physical Review Fluids*, 1(3):032402, 2016.

Berend Snijder and Lucas Pelkmans. Origins of regulated cell-to-cell variability. *Nature reviews Molecular cell biology*, 12(2):119–125, 2011.

Sabrina L Spencer, Suzanne Gaudet, John G Albeck, John M Burke, and Peter K Sorger. Non-genetic origins of cell-to-cell variability in trail-induced apoptosis. *Nature*, 459(7245):428–432, 2009.

David W Sroczynski, Felix Dietrich, Eleni D Koronaki, Ronen Talmon, Ronald R Coifman, Erik Bollt, and Ioannis G Kevrekidis. On learning what to learn: heterogeneous observations of dynamics and establishing (possibly causal) relations among them. *arXiv preprint arXiv:2406.06812*, 2024.

Martin P Stewart, Armon Sharei, Xiaoyun Ding, Gaurav Sahay, Robert Langer, and Klavs F Jensen. In vitro and ex vivo strategies for intracellular delivery. *Nature*, 538(7624):183–192, 2016.

Floris Takens. Estimation of dimension and order of time series. In *Nonlinear dynamical systems and chaos*, pp. 405–422. Springer, 1996.

Ali Tavasoli, Behnaz Moradijamei, and Heman Shakeri. Characterizing the load profile in power grids by koopman mode decomposition of interconnected dynamics. *arXiv:2304.07832v1*, 2023. doi: https://doi.org/10.48550/arXiv.2304.07832. URL `https://arxiv.org/abs/2304.07832`.

Claire Valva and Dimitrios Giannakis. Physics-informed spectral approximation of koopman operators. *arXiv preprint arXiv:2408.05663*, 2024.

Caleb Weinreb, Samuel Wolock, Betsabeh K Tusi, Merav Socolovsky, and Allon M Klein. Fundamental limits on dynamic inference from single-cell snapshots. *Proceedings of the National Academy of Sciences*, 115(10):E2467–E2476, 2018.